In-line spin torque nano-oscillators in perpendicularly magnetized nanowires

In-line spin-torque nano-oscillators in perpendicularly magnetized nanowires

R. A. van Mourik,[1,2,*] T. Phung,[1] S. S. P. Parkin,[1] and B. Koopmans[2]
[1]*IBM Almaden Research Center, San Jose, California 95120, USA*
[2]*Eindhoven University of Technology, Eindhoven, The Netherlands*
(Received 3 March 2015; revised manuscript received 19 November 2015; published 25 January 2016)

We propose a scheme for an in-line spin-torque nano-oscillator (iSTNO) composed of a single nanowire. The oscillating element is an in-plane magnetized region of an otherwise out-of-plane magnetized nanowire, which supports a spin-wave mode. Analytical exploration reveals that the nonadiabatic spin-transfer torque can cancel out the damping and thus induce sustained precession in response to a direct current. Moreover, it predicts that the frequency scales linearly with current and that the wave vector depends only on geometry. Simulations with single iSTNO cells confirm that oscillations occur, and simulations with two iSTNO cells show that they frequency lock to each other roughly in antiphase, even with mismatches in geometry. iSTNO devices can be easily fabricated by irradiating regions of a perpendicular magnetic anisotropy nanowire with ions, do not require an external field, inherently support multiple iSTNOs, and thus form an attractive alternative STNO.

DOI: 10.1103/PhysRevB.93.014435

I. INTRODUCTION

One of the envisioned applications accompanying the discovery of spin-transfer torque (STT) [1] was sustained precession of a magnetic layer induced by spin-polarized direct current; the prediction has resulted in the emergence of the field of *spin-torque nano-oscillators* (STNOs) as an active area of spintronics research, with applications in communications, for example. Typically, STNOs comprise two magnetic layers separated by a nonmagnetic layer. Electrons in a direct current between the layers become spin polarized by the magnetic layer that has fixed magnetization, and they deposit their spin angular momentum in the other magnetic layer, exerting a torque on its free magnetization. Given large enough current, the STT can offset the inherent damping of the free layer moment's precession around an applied magnetic field and thus induce sustained oscillation. Because of giant or tunnel magnetoresistance exhibited by the multilayer, the oscillation of the free layer moment relative to the fixed layer moment translates into an oscillating voltage that typically lies in the microwave (GHz) range.

STNOs have the potential to replace complementary metal-oxide semiconductor (CMOS)-based oscillators in communication applications for reasons that include their small size and ready tunability by current and applied magnetic field. However, obstacles to their application include their low output power as well as their need for a large applied magnetic field. Some alternative geometries [2] address the latter, but they carry fabrication challenges. Methods to increase STNO power output include higher magnetoresistance and larger precession angle within magnetic tunnel junction (MTJ) or nanocontact (NC) STNOs, or by turning to vortex (V) STNOs, but practical devices will nevertheless likely require synchronization of multiple STNOs to achieve useful power outputs. To date, only three NC STNOs [3,4] and four V STNOs [5] have been shown to oscillate coherently.

We present an alternative geometry of STNOs: the in-line STNO (iSTNO), where in-plane–anisotropy regions (cells) of an otherwise out-of-plane magnetized nanowire oscillate in response to a direct current. The device does not need an external magnetic field, extension to multiple coupled cells is built in, and fabrication is simpler than conventional STNOs. In this paper, we introduce the concept of the iSTNO, present an analytical model to explain its operation and make predictions, and show simulation results of one- and two-cell devices.

II. CONCEPT

The geometry of a single iSTNO starts with a magnetic nanowire with a thin rectangular cross section [see Fig. 1(a)]. It should have perpendicular magnetic anisotropy (PMA) so that the magnetization points out of plane (oop), except for a small region—a short longitudinal stretch of nanowire—without PMA. This "cell" constitutes the active iSTNO region. Here competition between in-plane shape anisotropy and exchange energy leaves the magnetization canted between the in-plane and out-of-plane directions. Simply sourcing a current through the nanowire introduces the necessary STT inside the cell. This excites a spin wave traveling along the nanowire length, made up of spins precessing around the out-of-plane direction. Since the wavelength typically exceeds the cell length, the average magnetization throughout the cell precesses with considerable amplitude, forming a magnetic oscillator.

The nanowire naturally supports multiple STNOs by having several no-PMA regions along the nanowire, separated by a short stretch of PMA nanowire [see Fig. 1(c)]. Moreover, the cells automatically couple to their neighbors through a combination of spin-wave and magnetostatic interactions; this means that they phase lock, forming a synchronized array of STNOs, which generally leads to amplified signal and reduced linewidth [6,7].

Notably, the iSTNO does not require an external magnetic field because the cells' magnetization precesses around a built-in field: magnetostatic fields from the PMA regions accumulate to a field across each cell that is antiparallel to the PMA magnetization.

To implement the scheme in practice, one would pattern nanowires from a PMA material such as Co/Ni bilayers [8] that

*r.a.v.mourik@alumnus.tue.nl

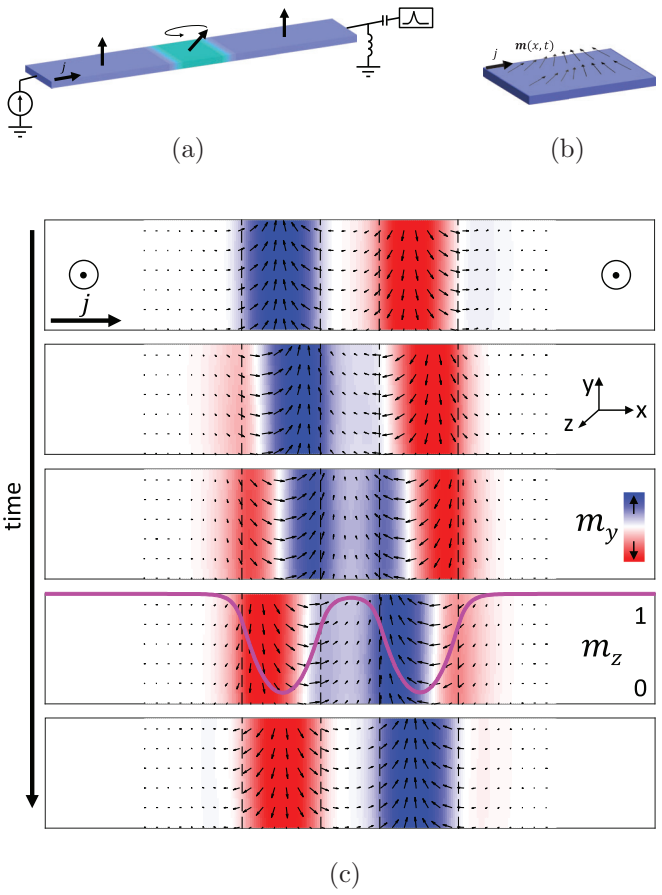

FIG. 1. (a) Schematic of the in-line spin-torque nano-oscillator (iSTNO). A region without PMA of an otherwise PMA nanowire precesses in response to direct current, around magnetostatic field lines from the out-of-plane regions. A spectrum analyzer measures the oscillation through a bias tee. (b) Geometry of the analytical model. Only the in-plane region is considered, and a one-dimensional spin wave is taken as ansatz. (c) Snapshots of a half period of oscillation of two iSTNOs. The PMA nanowire (here with cross section 60×1 nm^2) has regions (here, 40 nm long; dotted lines) without out-of-plane anisotropy. Color denotes the transverse component of magnetization, and the line in the fourth image depicts the z component of (unit) magnetization averaged across the cross section. Note that the cells are synchronized nearly in antiphase.

are a few nm thick and a few tens of nm wide. Regions of the nanowire, which are a few tens of nm long, can be stripped of their PMA using ion irradiation, either by a focused ion beam [9] or by irradiating through patterned resist [10]; the correct dose of ion irradiation destroys most of the magnetocrystalline anisotropy while leaving most of the magnetization intact. The method extends trivially to multiple STNOs. Contacts on either end of the nanowire establish the current source.

The contacts doubly serve as output: through the anisotropic magnetoresistance (AMR) effect, the resistance across the cell oscillates [at double the STNO frequency since the resistance change $\delta\rho \propto m_x^2 \propto \cos^2(\omega t)$], which with a constant current translates into an oscillating voltage that can be separated from the source current through a bias tee.

III. ANALYTICAL MODEL

To explain the oscillation in the iSTNO geometry and to understand how to tune the oscillation frequency, we start with a model that reduces the system to just the iSTNO cell: a single thin rectangular prism without PMA [see Fig. 1(b)]. That is, the PMA regions no longer adjoin the STNO cell, so there is no 90° domain wall, and the perpendicular magnetization component m_z is uniform across the cell. The PMA region's role as the source of magnetostatic field is included in the model in the perpendicular component of the dipolar field.

The other starting point is the Landau-Lifshitz-Gilbert (LLG) equation with STT terms, for one-dimensional unit magnetization $\mathbf{m}(x,t)$ and current in the x direction:

$$\frac{d\mathbf{m}}{dt} = -|\gamma|\mathbf{m} \times \mathbf{H}_{\text{eff}} + \alpha\mathbf{m} \times \frac{d\mathbf{m}}{dt} - u\frac{d\mathbf{m}}{dx} + \beta u\mathbf{m} \times \frac{d\mathbf{m}}{dx}, \tag{1}$$

with γ the gyromagnetic ratio, α the Gilbert damping constant, u the adiabatic STT magnitude, and β the nonadiabatic STT term. Furthermore, u relates directly to current density j by

$$u = \frac{g\mu_B P}{2|e|M_s} j, \tag{2}$$

with g the Landé factor, μ_B the Bohr magneton, P the electron polarization, e the electron charge, and M_s the saturation magnetization. $\mathbf{H}_{\text{eff}}$ includes the effective exchange field and dipolar field,

$$\mathbf{H}_{\text{eff}} = \mathbf{H}_{\text{exch}} + \mathbf{H}_{\text{dip}} = \frac{2A}{\mu_0 M_s^2}\frac{d^2\mathbf{m}}{dx^2} + \mathbf{H}_{\text{dip}}, \tag{3}$$

where A is the exchange stiffness and $\mathbf{H}_{\text{dip}}$ is further discussed below.

As ansatz for $\mathbf{m}$, we take the profile of a one-dimensional spin wave traveling in the wire direction $\hat{\mathbf{x}}$, its spins precessing with amplitude ρ around the out-of-plane direction $\hat{\mathbf{z}}$:

$$\mathbf{m}(x,t) = \begin{pmatrix} \rho\cos(kx - \omega t) \\ \rho\sin(kx - \omega t) \\ \sqrt{1-\rho^2} \end{pmatrix}. \tag{4}$$

After $\mathbf{m}$ [Eq. (4)] is substituted into the LLG equation (1), analysis of the resulting terms on the right side of the equation reveals the presence of all ingredients of an auto-oscillator [11], namely, (i) an effective field around which to precess, (ii) natural damping, and, most distinctively, (iii) opposition to this damping, or *antidamping*. The field from the PMA regions, adiabatic STT term, and exchange all produce terms parallel to $d\mathbf{m}/dt$ (the direction of precession), resembling an oop field around which the magnetization can revolve (i), and the usual damping term $\alpha\mathbf{m} \times d\mathbf{m}/dt$ (ii) tends to reduce that precession in favor of alignment with $\mathbf{H}_{\text{eff}}$. Crucially, the nonadiabatic term, $\beta u\mathbf{m} \times d\mathbf{m}/dx$, evaluates to a vector antiparallel to the damping (iii), away from $\mathbf{H}_{\text{eff}}$; with large enough current, this term offsets the natural damping and the system undergoes sustained oscillation.

The dipolar field $\mathbf{H}_{\text{dip}}$ [Eq. (3)] helps to determine the frequency, critical current, and amplitude, but, as usual, it eludes a simple form and necessitates approximation and numerical evaluation. Here two consequences of the cell's membership of the full nanowire system are taken into consideration:

(a) the PMA regions' magnetostatic field contributes to the total dipole field, and (b) the spin wave is not strongly pinned at the longitudinal cell boundaries, so free boundary conditions are assumed.

The z component of the dipolar field within the cell, $H_{\mathrm{dip},z}$, consists of contributions from the PMA regions (H_{PMA}) and the cell itself ($-M_s N_z m_z$). It can be modeled as uniform using formulas for rectangular prisms [12,13]. When compared with the true $H_{\mathrm{dip},z}$ as calculated using a magnetostatic Green's function [14], the uniform assumption holds up well everywhere in the cell except at the edges, as shown in Fig. 5.

For a suitable approximation of the x and y components of H_{dip}, we take the dipolar field of a spin wave extending in an infinite wire, crop this to a finite cell, and correct the proportionality factor by comparing it to the x and y components of the true dipolar field. In an infinite wire, given the one-dimensional magnetization profile $m_x \propto \cos(kx - \omega t)$ and $m_y \propto \sin(kx - \omega t)$ as in Eq. (4), the x and y components of the one-dimensional dipolar field are themselves traveling waves, exactly represented by $H_{\mathrm{dip},x}(x) \propto m_x$ and $H_{\mathrm{dip},y}(x) \propto m_y$. In the finite cell, we use these expressions to approximate the dipolar field.

The proportionality factors are chosen to best approximate the true dipolar field within the finite cell over an oscillation period, and they depend on k (see Appendix for details). Thus, we write $H_{\mathrm{dip},x}(x) = -M_s N_x(k) m_x(x)$ and $H_{\mathrm{dip},y}(x) = -M_s N_y(k) m_y(x)$. For $k = 0$, these expressions reproduce the average self-magnetostatic field of a uniformly magnetized rectangular prism [13]. As $k \to \infty$, $N_x(k) \to 1$ and $N_y(k) \to 0$.

Just as the $H_{\mathrm{dip},z}$, this approximation for $H_{\mathrm{dip},x}$ and $H_{\mathrm{dip},y}$ works well away from the edges, as shown in Fig. 5. The accuracy also varies throughout an oscillation period, but this is significant only for values of k around π/L, where L is the length of the cell along the x direction. Including a correction for this into $H_{\mathrm{dip},x}$ and $H_{\mathrm{dip},y}$ is possible, but is too much detail for the model to be able to still make predictions.

In total, the dipolar field is modeled as

$$\mathbf{H}_{\mathrm{dip}}(x) = -M_s \begin{pmatrix} N_x(k) \\ N_y(k) \\ N_z \end{pmatrix} \circ \mathbf{m}(x) - H_{\mathrm{PMA}}\hat{\mathbf{z}}, \qquad (5)$$

where $\circ$ denotes elementwise multiplication.

The expression for $\mathbf{H}_{sm}$ [Eq. (5)] completes the substitutions to the LLG equation (1). After simplifying, it leaves three linear relations (one for each component) with $\cos(kx - \omega t)$, $\sin(kx - \omega t)$, and $\sin(kx - \omega t)\cos(kx - \omega t)$ terms. To make the equation valid for all t, the coefficients of these terms are set to zero, and we find that the following relations must hold:

$$N_x(k) = N_y(k), \qquad (6)$$

$$\omega = \frac{\beta}{\alpha} k u. \qquad (7)$$

The first determines the wave number k and states that it depends only on the geometry of the cell. It also requires that the cell be wider than it is long. The second expresses the dispersion relation of the system and reveals that current linearly tunes the frequency.

IV. SIMULATIONS

We used the OOMMF micromagnetic simulator [15] to confirm that iSTNO cells oscillate and to determine the effect on frequency and critical current of various parameters, such as cell dimensions, α, and β. For simulations of nanowires with single cells, cell length varied from 20 to 60 nm, wire width 20–60 nm, wire thickness 1–5 nm, α spanned 0.01–0.05, and β spanned 0–0.04. The magnetocrystalline anisotropy transitioned abruptly from 3.5×10^5 J/m^3 in the PMA regions to 0 in the cells. In addition, the simulations included a small field consisting of randomly oriented vectors of magnitude, usually 80 A/m at each point in the mesh throughout the nanowire to break symmetry and represent inhomogeneities, and their magnitude also varied by a decade each direction to evaluate their influence on performance. The current applied to the wire increased stepwise.

Simulations successfully demonstrate the anticipated behavior of the iSTNO cell: above a critical current, an approximately one-dimensional spin wave appears in each cell; Fig. 1(c) shows snapshots of a simulation with two cells during their oscillation. The magnetization profile matches Eq. (4) with only the substitution $\rho \to \rho(x)$; the line in the fourth image of Fig. 1(c) shows that m_z deviates from uniformity.

Figure 2 shows a typical power spectrum of a simulation of a nanowire with a single cell, where the current density increases from $j = 1$ to 25×10^{12} A/m^2. Two spectra at each current correspond to the average m_x and m_y averaged over the cell; note that they coincide for currents where oscillation occurs. For the shown configuration, i.e., a cell of dimensions $40 \times 60 \times 1$ nm^3 with $\alpha = 0.04$ and $\beta = 0.04$, we find that frequency increases linearly with current, and this is true for almost all simulations where oscillations occur, some of which are detailed in the inset of Fig. 2. Simulations where $\beta = 0$ did not oscillate, as prohibited by the analytical model. The critical current does not depend on various parameters in a simple way, although the lowest currents—down to 4×10^{12} A/m^2—are found in simulations where $\beta = 0.04$ and $\alpha = 0.01$.

The second claim—of automatic coupling and synchronization of multiple iSTNO cells on one nanowire—also comes under test through simulation, quite simply by setting the PMA of a second region to 0. Additional parameters come into play: the spacing between cells and the mismatch between the cell lengths. We observe whether oscillation and synchronization are sensitive to differences between the STNOs' dimensions and corresponding natural frequencies. Recall that the snapshots in Fig. 1(c) feature two cells oscillating together nearly in antiphase. Indeed, when a second cell, with slightly different length, is added in the configuration of Fig. 2, spectra of m_x and m_y for both cells coincide up to a certain current, above which they decouple (Fig. 3).

The cell lengths of the shown configuration are actually mismatched by 10%—they are 40 and 44 nm long, respectively—and separated by 50 nm PMA region. In fact, coupled oscillations were observed for all simulations, with the second cell length varying from 36–44 nm and the spacing from 20–80 nm, attesting to the robustness of the coupling mechanism, although they decoupled at high currents with large separations (see inset of Fig. 3). Moreover, both

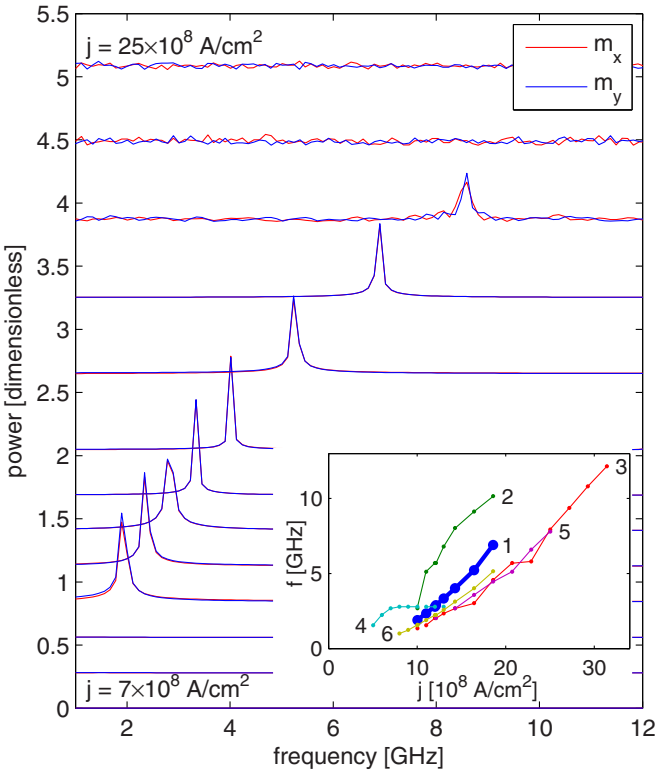

FIG. 2. Typical simulation result: spectra of oscillations of an STNO cell of dimensions $40 \times 60 \times 1$ nm^3, with $\alpha = 0.04$ and $\beta = 0.04$. Spectra are taken from the average m_x and m_y across the cell. The inset shows frequency vs current density for a selection of simulations: "1": (bold) same parameters; "2": $60 \times 60 \times 5$ nm^3, $\alpha = 0.02$, $\beta = 0.04$; "3": $20 \times 60 \times 5$, 0.05, 0.04; "4": $20 \times 60 \times 5$, 0.01, 0.04; "5": $20 \times 40 \times 5$, 0.05, 0.04; and "6": $20 \times 60 \times 1$, 0.05, 0.04.

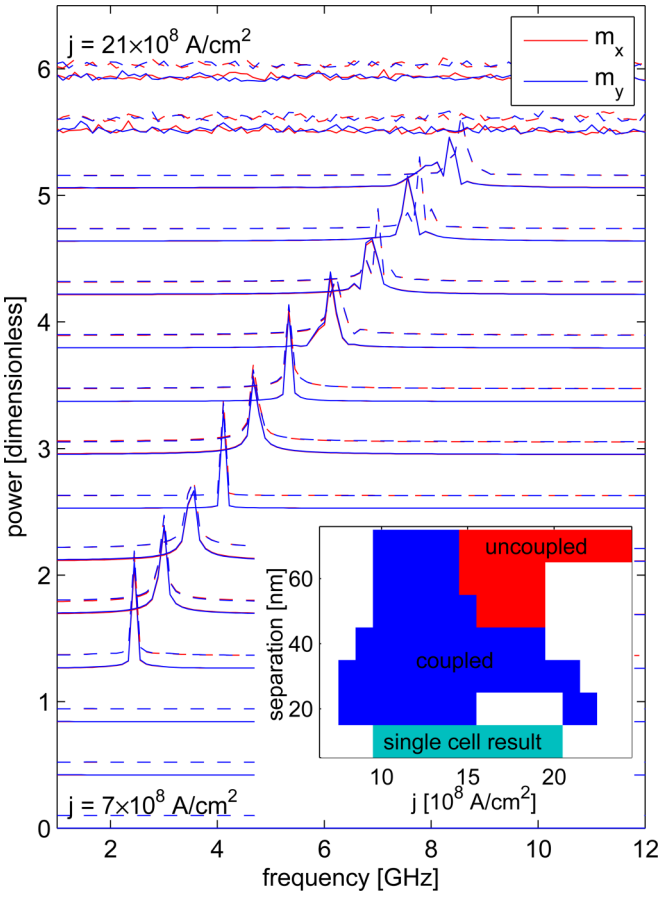

FIG. 3. Simulation results of two iSTNO cells of dimensions $40 \times 60 \times 1$ nm (solid lines) and $44 \times 60 \times 1$ nm (dotted lines, offset for clarity), separated by 50 nm, with $\alpha = 0.04$ and $\beta = 0.04$. Their oscillations are coupled. The inset shows the occurrence of successful oscillation (the single-cell result is provided for comparison).

cells oscillate with slightly higher power than their single-cell counterpart. Finally, the phase difference between the oscillations in this case depends linearly on current. This is because the spin wave extends through the PMA region (even though the amplitude there is nearly 0) and the wave number has a linear relation to current. That said, the phase difference tends to stay within $\pi/2$ and $3\pi/2$ for all tested configurations with various cell lengths and separations that are $\leqslant$50 nm over the range of currents at which oscillations occur, staying much closer to π in some cases even. This may imply dipolar coupling between cells, specifically favoring the configuration where the average magnetizations of the two cells are in the $+y$ and $-y$ directions, respectively. However, dipolar coupling promotes different phase differences at every point during the cells' oscillations, for example the zero phase difference between simultaneous $+x$ and $+x$ magnetizations (also $-x$ and $-x$), but it appears that the $+y$ and $-y$ coupling dominates. In short, the phase difference likely arises from a combination of spin-wave continuation and dipolar coupling, but further research should determine the exact mechanism. Since coupling has considerable range (evident from frequency locking at large separations), coupling between nonadjacent cells must also be considered, but whether it is significant and constructive depends on the underlying mechanism.

V. DISCUSSION

We test the accuracy of the model described in Sec. III by extracting the frequency and wave numbers of the spin waves from simulation iSTNO cells and comparing them against predictions by Eqs. (6) and (7). Starting with the dispersion [Eq. (7)], Fig. 4(a) displays the wave number versus frequency from simulations with various parameters and currents, and the inset details this for some values of α. Strong agreement of the data with the lines in the figure, which represent Eq. (7), verifies the dispersion predicted by the model.

From a glance at the wave numbers extracted from simulations by themselves, however, it appears that they vary approximately linearly with current [see Fig. 4(b)], in sharp contrast to the prediction that they should depend only on the cell geometry [Eq. (6)]. In fact, there is no solution to Eq. (6) if the cell is wider than it is long, whereas some geometries with this condition oscillate nonetheless [e.g., curves "3" and "6" in Fig. 4(b)]. Here, the limitation of the simplicity of the model appears: the domain walls between the PMA and no-PMA regions, neglected in the model, play an important role in determining the wave number (and thus the frequency.) For one, the spin wave can extend throughout the domain wall, i.e., beyond the cell's edges, effectively lengthening the cell,

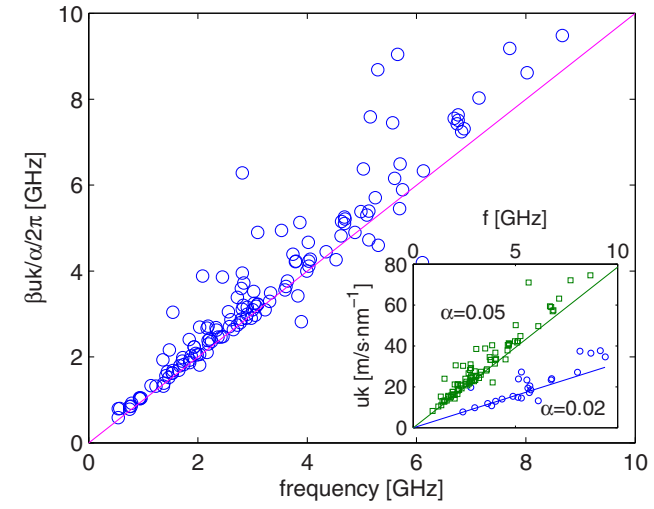

(a)

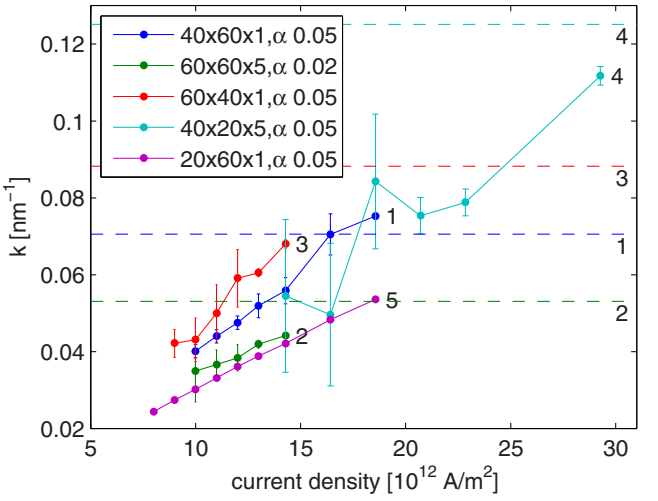

(b)

FIG. 4. (a) Frequency vs wave number extracted from simulations of various geometries, α, β, and currents. Wave numbers k are normalized by α, β, and u for comparison to frequency, and the line represents equality [cf. Eq. (7)], and the inset details this for cases where $\beta = 0.04$ and $\alpha = 0.02$ or 0.05. (b) Wave number vs current for selected simulations. Dotted lines represent the prediction [Eq. (6)].

countering the aforementioned condition that disqualified a solution for the wave number. Furthermore, since dm_z/dx is no longer 0, the terms in the LLG equation (1) containing $d\mathbf{m}/dx$ gain additional character. The adiabatic STT term has the well-known effect of propagating the domain walls [16], which in the case of bound domain walls means they merely shift along the nanowire. The nonadiabatic term has the more interesting effect of rotating the magnetization counterclockwise in the left domain wall and clockwise in the right one. Competing against exchange and magnetostatic forces, this leads to a phase difference across the cell, suggesting an avenue for a new wave-number prediction. Moreover, since these terms depend on u, this prediction would depend on current, consistent with simulation results as in Fig. 4(b).

It turns out that the wave number depends on current, even if the domain walls are removed from the simulation by considering only the no-PMA region. This exposes the limitation of the approximation made for the self-magnetostatic field [Eq. (5)]. Because, in general, the wave number $k \lesssim \pi/L$, the finite size of the cell causes considerable deviations, especially at the cell's edges (were $k \gg \pi/L$, the edge effects would become negligible). The presence of a nonzero dm_z/dx then introduces similar effects as before, and notwithstanding the smaller magnitude of dm_z/dx, the much larger currents required to oscillate a lone cell render the whole nonadiabatic term $\beta u\mathbf{m} \times d\mathbf{m}/dx$ quite relevant. The higher currents necessary in the absence of PMA regions furthermore suggest that the domain walls also serve to reduce the critical current, either by priming the phase difference across the cell as previously explained or by precession of the domain wall itself [17].

As a final note, the random field introduced some variance in the wave vector for some configurations and currents [see error bars in Fig. 4(b)]. On the other hand, the frequency and critical current are not affected, suggesting that the oscillations are resistant to inhomogeneities or, in other words, are not limited to ideal conditions.

VI. CONCLUSION

We have presented an alternative geometry for a spin-torque nano-oscillator, where the active elements are in-plane magnetized regions of an otherwise out-of-plane magnetized nanowire, and have shown simulation results that confirm oscillations in these cells. Multiple cells oscillate in coupled fashion, resistant to size mismatches. A theoretical model based on a spin wave in solely the in-plane region correctly identifies the dispersion relation that simulations also produced. Despite some of the model's assumptions, such as uniform amplitude, uniform field from the out-of-plane regions, and an approximation for the self-magnetostatic field, it correctly derives the wave vector's order of magnitude but misses its current dependence.

Section II touched upon fabrication and circuitry of a physical iSTNO device. Experiments are in progress to demonstrate the phenomenon in real nanowires, but some challenges need to be addressed. First, the required current densities in simulation in most cases equate to a few mA of current, comparable to the breaking threshold of the nanowires, so experiments are limited to parameters with the lowest critical currents. Although several parameters were varied during the simulation study, a thorough exploration of the parameter space is left for further research. Generally, the simulations that produced the highest amplitude oscillations with the lowest critical current densities had a large difference between anisotropy constants of the PMA and oscillation regions, a very thin wire, and a high value of the nonadiabatic parameter β. The latter reflects the analytical result that the nonadiabatic STT term in the LLG equation constitutes antidamping necessary for the onset of oscillation.

Second, when testing single iSTNO and relying on AMR as output, the resulting oscillating voltage is rather small [and since the amplitude is proportional to $\sin(kL)/kL$, it may vanish entirely if kL is a multiple of π]. However, we estimate that the amplitude can be of the order of 10 μV, which is easily discernible from noise on spectrum analyzers. Another method to measure small oscillations is the spin-diode technique [18].

As a final note, the analytical model discards the out-of-plane section of the nanowire and mimics its magnetostatic contribution by an equivalent field, so the iSTNO can alternatively be built as magnetic in-plane sections within an otherwise nonmagnetic nanowire subjected to an external field. In fact, since the exchange and (approximately) the self-magnetostatic fields appear in the equations as contributions to the effective field, an external field may not be necessary in some configurations. However, the required currents are much higher, and fabrication of practical devices would come with challenges not present in the PMA-nanowire-based iSTNO.

ACKNOWLEDGMENT

This work is supported by NanoNextNL, a micro and nanotechnology program of the Dutch Government and 130 partners.

APPENDIX: DIPOLAR FIELD APPROXIMATION

In Sec. III, we presented an approximation of the dipolar field that results from the magnetization profile given by

$$\mathbf{m}(x,t) = \begin{pmatrix} \rho\cos(kx-\omega t) \\ \rho\sin(kx-\omega t) \\ \sqrt{1-\rho^2} \end{pmatrix}. \qquad \text{(4 rep.)}$$

The approximation reads

$$\mathbf{H}_{\text{dip}}(x) = -M_s \begin{pmatrix} N_x(k) \\ N_y(k) \\ N_z \end{pmatrix} \circ \mathbf{m}(x) - H_{\text{PMA}}\hat{\mathbf{z}}, \qquad \text{(5 rep.)}$$

where $\circ$ denotes elementwise multiplication. Here we compare this with the true dipolar field, as calculated using magnetostatic Green's functions [14]. As a sample case, we take

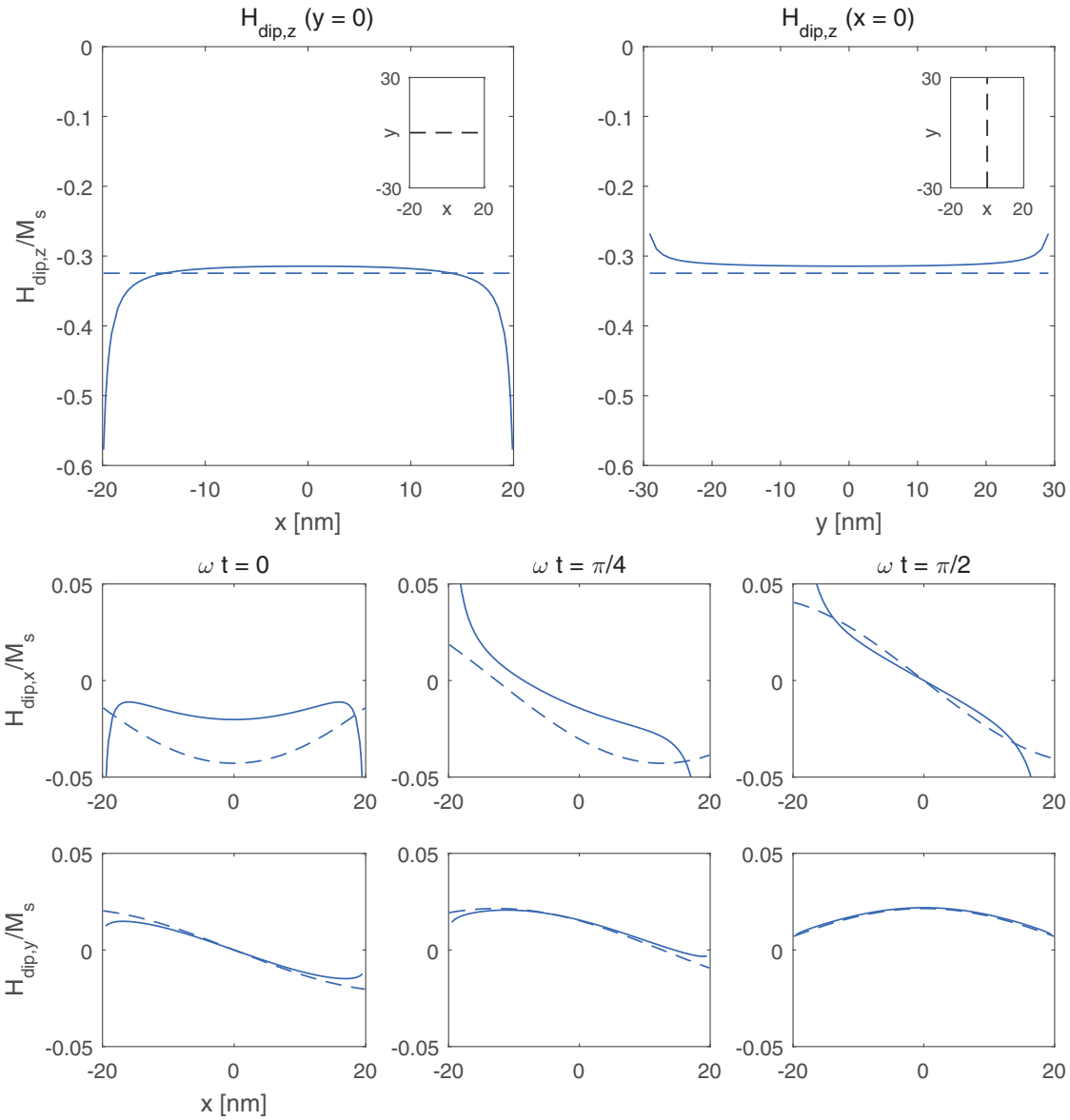

FIG. 5. True dipolar field (solid lines) and its approximation (dashed lines) for a rectangular element of size $40 \times 60 \times 1$ nm^3 carrying a spin-wave magnetization profile with wave vector 0.06 nm^{-1}. The top plots show lineouts of $H_{\text{dip},z}$ along $x = 0$ and $y = 0$, averaged over the out-of-plane coordinate z. The bottom plots show $H_{\text{dip},x}(x)$ and $H_{\text{dip},y}(x)$, averaged over y and z.

a $40 \times 60 \times 1$ nm^3 cell oscillating with $k = 0.06$ nm^{-1} and $\rho = 0.95$, as in Figs. 1(c) and 2.

The z component, $H_{\mathrm{dip},z}$, is modeled as uniform and sums the contributions from the magnetization of the cell itself and the PMA regions. We compare this with the true dipolar field of a nanowire with magnetization inside the cell and fully out-of-plane magnetization everywhere else. Lineouts of the true and approximate dipolar field at $x = 0$ and $y = 0$ are plotted in Fig. 5. Away from the edges, the uniform approximation is justified.

The x and y approximations include factors N_x and N_y that depend on k. They are calculated by extracting the coefficient of $\cos(kx - \omega t)$ or $\sin(kx - \omega t)$ from the true dipolar field averaged over the transverse and perpendicular coordinates y and z, $\mathbf{H}_{\mathrm{dip,true}}(x)$, and averaging over an oscillation period:

$$\mathbf{N}(k) = -\frac{1}{\rho^2 M_s}\frac{1}{2\pi/\omega}\int_0^{2\pi/\omega}\frac{2}{L}\int_{-L/2}^{L/2}\mathbf{H}_{\mathrm{dip,true}}(x)\circ\mathbf{m}(x)dxdt, \tag{A1}$$

for $\mathbf{N}(k) = [N_x(k), N_y(k)]$.

Figure 5 shows the approximations as well as the true dipolar field. $H_{\mathrm{dip},y}$ matches the true field except near the edges. $H_{\mathrm{dip},x}$ underestimates the true field at parts of an oscillation period, but overestimates it at other times so that the amplitude averages correctly. At the edges, $H_{\mathrm{dip},x}$ and $H_{\mathrm{dip},y}$ neglect the pinning at the longitudinal edges of the rectangular element, but free boundary conditions do reflect the behavior in the system we are modeling, i.e., a cell lifted from a nanowire.

The approximations thus capture the oscillating nature in time and space of the x and y components of the dipolar field, but the accuracy varies throughout an oscillation. However, since $H_{\mathrm{dip},x}$ and $H_{\mathrm{dip},y}$ are small compared with $H_{\mathrm{dip},z}$ and the other terms in the equation, this is negligible. In fact, this approximation enables making a prediction of the wave vector k, while a more detailed approximation would lead to overdetermination and failure of the model to make predictions.

[1] J. C. Slonczewski, Current-driven excitation of magnetic multilayers, J. Magn. Magn. Mater. **159**, L1 (1996).

[2] C. Fowley, V. Sluka, K. Bernert, J. Lindner, J. Fassbender, W. H. Rippard, M. R. Pufall, S. E. Russek, and A. M. Deac, Zero-field spin-transfer oscillators combining in-plane and out-of-plane magnetized layers, Appl. Phys. Express **7**, 043001 (2014).

[3] M. Hiroki, K. Hitoshi, S. Yoshishige, S. Takayuki, N. Kazumasa, N. Yoshinori, T. Koji, F. Akio, M. D. Alina, A. Koji, and Y. Shinji, Large emission power over 2 W with high Q factor obtained from nanocontact magnetic-tunnel-junction-based spin torque oscillator, Appl. Phys. Express **6**, 113005 (2013).

[4] S. Sani, J. Persson, S. M. Mohseni, Y. Pogoryelov, P. K. Muduli, A. Eklund, G. Malm, M. Kall, A. Dmitriev, and J. Akerman, Mutually synchronized bottom-up multi-nanocontact spintorque oscillators, Nat. Commun. **4**, 2731 (2013).

[5] A. Ruotolo, V. Cros, B. Georges, A. Dussaux, J. Grollier, C. Deranlot, R. Guillemet, K. Bouzehouane, S. Fusil, and A. Fert, Phase-locking of magnetic vortices mediated by antivortices, Nat. Nanotechnol. **4**, 528 (2009).

[6] S. Kaka, M. R. Pufall, W. H. Rippard, T. J. Silva, S. E. Russek, and J. A. Katine, Mutual phase-locking of microwave spin torque nano-oscillators, Nature (London) **437**, 389 (2005).

[7] F. B. Mancoff, N. D. Rizzo, B. N. Engel, and S. Tehrani, Phase-locking in double-point-contact spin-transfer devices, Nature (London) **437**, 393 (2005).

[8] M. Haertinger, C. H. Back, S. H. Yang, S. S. P. Parkin, and G. Woltersdorf, Properties of Ni/Co multilayers as a function of the number of multilayer repetitions, J. Phys. D **46**, 175001 (2013).

[9] R. Hyndman, P. Warin, J. Gierak, J. Ferre, J. N. Chapman, J. P. Jamet, V. Mathet, and C. Chappert, Modification of Co/Pt multilayers by gallium irradiationPart 1: The effect on structural and magnetic properties, J. Appl. Phys. **90**, 3843 (2001).

[10] C. Chappert, H. Bernas, J. Ferr, V. Kottler, J. P. Jamet, Y. Chen, E. Cambril, T. Devolder, F. Rousseaux, V. Mathet, and H. Launois, Planar patterned magnetic media obtained by ion irradiation, Science **280**, 1919 (1998).

[11] A. Slavin and V. Tiberkevich, Nonlinear auto-oscillator theory of microwave generation by spin-polarized current, IEEE Trans. Magn. **45**, 1875 (2009).

[12] M. Maicus, E. Lopez, M. C. Sanchez, C. Aroca, and P. Sanchez, Magnetostatic energy calculations in two- and three-dimensional arrays of ferromagnetic prisms, IEEE Trans. Magn. **34**, 601 (1998).

[13] A. Aharoni, Demagnetizing factors for rectangular ferromagnetic prisms, J. Appl. Phys. **83**, 3432 (1998).

[14] K. Y. Guslienko and A. N. Slavin, Magnetostatic greens functions for the description of spin waves in finite rectangular magnetic dots and stripes, J. Magn. Magn. Mater. **323**, 2418 (2011).

[15] M. Donahue and D. Porter, *OOMMF User's Guide, Version 1.0*, Interagency Report NISTIR 6376 (National Institute of Standards and Technology, Washington, D.C., 1999).

[16] L. Thomas and S. Parkin, Current induced domain-wall motion in magnetic nanowires, in *Handbook of Magnetism and Advanced Magnetic Materials*, Vol. 2, edited by H. Kronmüller and S.S.P. Parkin (Wiley, New York, 2007), pp. 942–982.

[17] J. H. Franken, R. Lavrijsen, J. T. Kohlhepp, H. J. M. Swagten, and B. Koopmans, Tunable magnetic domain wall oscillator at an anisotropy boundary, Appl. Phys. Lett. **98**, 102512 (2011).

[18] A. A. Tulapurkar, Y. Suzuki, A. Fukushima, H. Kubota, H. Maehara, K. Tsunekawa, D. D. Djayaprawira, N. Watanabe, and S. Yuasa, Spin-torque diode effect in magnetic tunnel junctions, Nature (London) **438**, 339 (2005).